

**Phase Relations and Elemental Distribution among Co-Existing  
Phases in the Ceramics of the Pseudobinary System  $\text{CaZrTi}_2\text{O}_7\text{--CeAlO}_3$**

N.S. Mikhailenko, S.V. Stefanovsky  
SIA Radon,  
7<sup>th</sup> Rostovskii lane 2/14, Moscow 119121 RUSSIA, [profstef@mtu-net.ru](mailto:profstef@mtu-net.ru)

A.V. Ochkin  
D. Mendeleev University of Chemical Technology,  
Miuskaya sq. 9, Moscow 125047 RUSSIA, [ochkin@rctu.ru](mailto:ochkin@rctu.ru)

M.I. Lapina  
Institute of Geology of Ore Deposits, Mineralogy, Petrography and Geochemistry RAS,  
Staromonetnii lane 35, Moscow 109017 RUSSIA

**ABSTRACT**

Ceramics formally related to a pseudo-binary system  $\text{CaZrTi}_2\text{O}_7\text{--CeAlO}_3$  being important for design of matrices for immobilization of a rare-earth – actinide fraction of high level waste were synthesized by cold pressing and sintering at temperatures of 1400, 1450 and 1500 °C. It has been shown that the target zirconolite and perovskite structure phases as well as cerium and zirconium dioxide based cubic phases were formed. Content of the latter phases in the ceramics increases significantly with increase of sintering temperature to 1500 °C and they are capable to accumulate up to 77%  $\text{CeO}_2$  of total amount introduced.

**INTRODUCTION**

Pseudo-binary system  $\text{CaZrTi}_2\text{O}_7\text{--CeAlO}_3$  is of interest to analyzing cerium behavior in two-phase ceramics to be designed for immobilization of cerium-bearing rare earth – actinide (REE/An) fraction of high level waste (HLW). Moreover cerium is normally used as a plutonium surrogate and cerium-bearing systems are considered to be simulants at design of matrices for excess weapons plutonium immobilization.

Unlike lanthanum and most of different lanthanides cerium in ceramics may be present in both tri- and tetravalent forms depending on synthesis conditions and features of phase composition of the ceramics. Therefore phase relations in ceramics and cerium partitioning among co-existing phases may be rather complicated.

Investigations of cerium incorporation in the zirconolite structure in details [1-6] have shown that it may substitute for both calcium and zirconium in their sites by schemes:  $\text{Ca}^{2+} + \text{Ti}^{4+} = \text{Ce}^{3+} + \text{Me}^{3+}$  (Me = Al, Fe) and  $\text{Zr}^{4+} = \text{Ce}^{4+}$ . At coupled heterovalent substitution monoclinic structure (zirconolite-2M) is kept at low concentrations of  $\text{Ce}^{3+}$  ions (up to ~0.20-0.25 formula units – fu). Further substitution to ~0.5 fu transforms the structure to trigonal symmetry (zirconolite-3T). High cerium content results in formation of extra phases and fully Ce-

substituted zirconolite ( $\text{CeZrTiAlO}_7$ ) has not been obtained [6]. At isovalent substitution of  $\text{Zr}^{4+}$  for  $\text{Ce}^{4+}$  the structure is gradually transformed from monoclinic (2M) through intermediate variety (probably 4M) to cubic pyrochlore structure although as reported in ref. [3] a partial miscibility gap appears to exist in the pseudo-binary system  $\text{CaZrTi}_2\text{O}_7 - \text{CaCeTi}_2\text{O}_7$ . It is clear that complete transformation all the cerium in tetravalent or trivalent state requires strongly oxidizing or reducing conditions respectively. Normally at synthesis in air atmosphere both cerium states co-exist and its average oxidation state was found to be +3.5 [7].

In the perovskite-type phases cerium is preferably in a trivalent form. For cerium (III) aluminate –  $\text{CeAlO}_3$  rhombohedral (space group  $R\bar{3}m$  – ICDD-JCPDS 21-175) and cubic (ICDD-JCPDS 28-260) varieties are known.  $\text{CeFeO}_3$  relates to orthorhombic system and is isostructural with nominal perovskite  $\text{CaTiO}_3$ .

In accordance with crystal chemical behavior it can be expected that  $\text{Ce}^{4+}$  ions should enter zirconolite whereas  $\text{Ce}^{3+}$  ions would be partitioned among zirconolite and perovskite. However due to limited isomorphic capacity of the zirconolite with respect to cerium formation of extra phases like cerianite is probable [1,6]. The goal of the present work is identification of the phases possibly formed at ceramization of the REE/An fraction of HLW using cold pressing and sintering of oxide mixtures in air atmosphere at high temperatures and quantitative determination of elemental fractions entering various phases of the ceramics.

## EXPERIMENTAL

The ceramic samples with calculated compositions  $(1-x)\text{CaZrTi}_2\text{O}_7 - x\text{CeAlO}_3$  ( $x = 0.25, 0.5,$  and  $0.75$ ) were produced. Mixtures of oxides were milled and homogenized in a planetary mill AGO-2U (Russian design), compacted in pellets 5 mm in diameter and 3 mm in thickness, heat-treated stepwise in a resistive furnace to target sintering temperature (1400, 1450 or 1500 °C), kept at this temperature for 5 hours, and cooled down to room temperature in a turned-off furnace.

The samples were examined with X-ray diffraction using a Philips diffractometer and scanning electron microscopy with energy dispersive system (SEM/EDS) using a JSM-5300+Link ISIS analytical unit. Results of elemental microprobe analysis were recalculated to oxides assuming conventional valence states for Ca, Al, Ti, Zr, O and Ce valence (III) or (IV) in various systems from reference data.

## RESULTS AND DISCUSSION

In the system studied phase composition of ceramics depends strongly on synthesis temperature that may be explained by both increasing of solidus temperature at increase of perovskite constituent and variations in tri- and tetravalent cerium ratio.

As seen from XRD patterns (Figures 1-3) and SEM/EDS data (Figure 4) at 1400 °C phase formation reactions are completed only in the ceramic mixture with 0.75  $\text{CaZrTi}_2\text{O}_7 - 0.25\text{CeAlO}_3$  ( $x = 0.25$ ) formulation. This ceramic is composed of predominant zirconolite (80-85%), perovskite as a secondary in abundance phase (10-15%) and minor oxide phase (1-3%). Similar phase relation is in the ceramic with the same calculated composition sintered at 1450 °C.

Zirconolite in this sample has quite fixed composition and its chemical composition (Table I) is recalculated well to averaged formula  $\text{Ca}_{0.81}\text{Ce}_{0.24}\text{Zr}_{1.05}\text{Ti}_{1.60}\text{Al}_{0.28}\text{O}_7$ . As follows from charge balance three isomorphous substitution schemes are realized:  $\text{Ca}^{2+} + \text{Ti}^{4+} = \text{Ce}^{3+} + \text{Al}^{3+}$  (predominant),  $\text{Zr}^{4+} = \text{Ce}^{4+}$  (additional) и  $\text{Zr}^{4+} = \text{Ti}^{4+}$  (minor). Perovskite has more variable composition and averaged formula  $\text{Ca}_{0.70}\text{Ce}_{0.20}\text{Zr}_{0.03}\text{Ti}_{0.90}\text{Al}_{0.08}\text{O}_3$ . Chemical composition of oxide phase grains has not been determined due to fine grain size ( $< 1 \mu\text{m}$ ).

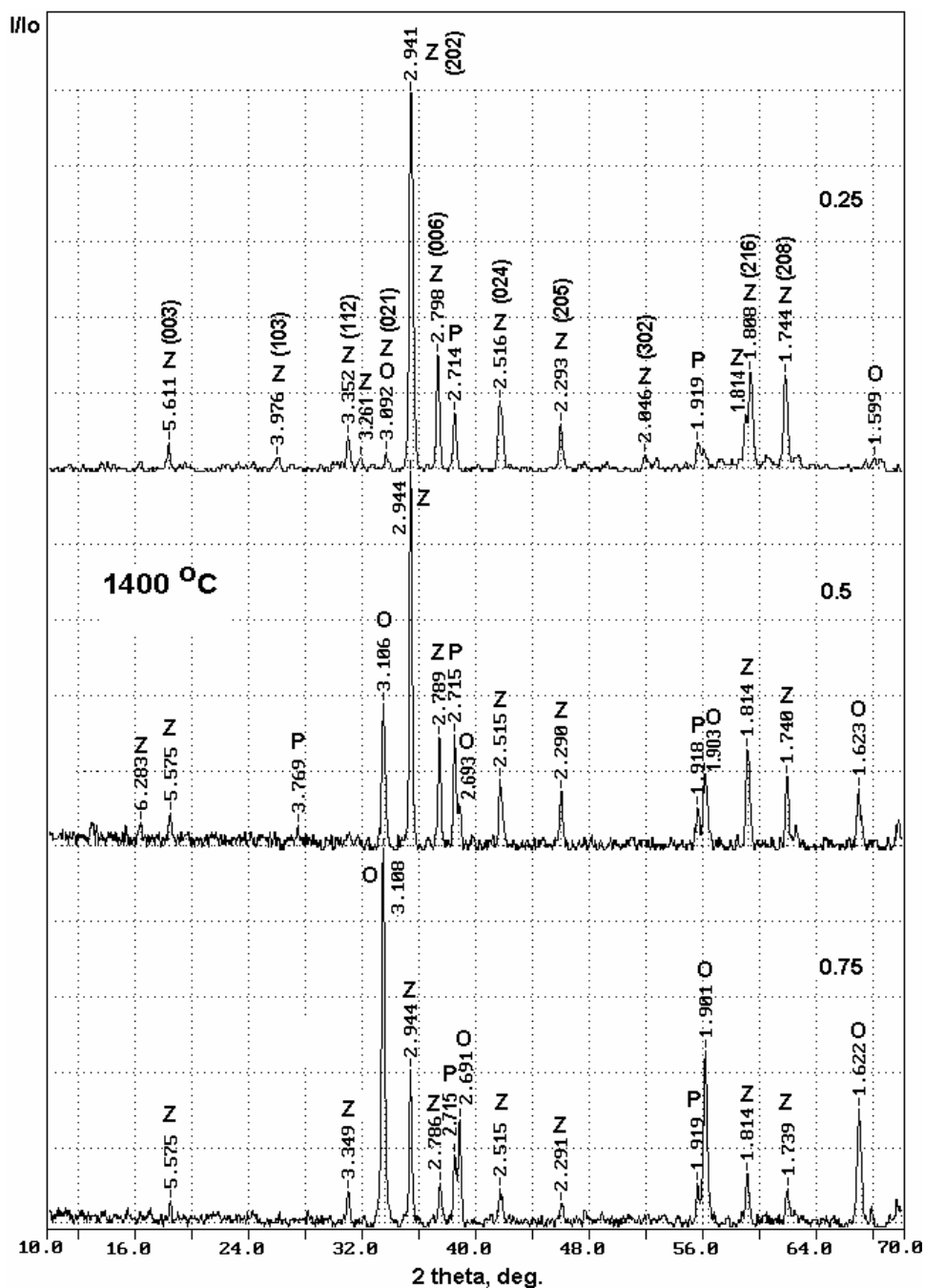


Fig. 1. XRD patterns of the ceramics in the series  $(1-x) \text{CaZrTi}_2\text{O}_7 - x \text{CeAlO}_3$  produced by sintering of pelletized oxide mixtures at  $1400 \text{ }^\circ\text{C}$ .

O – oxide phase, P – perovskite structure phase, Z – zirconolite

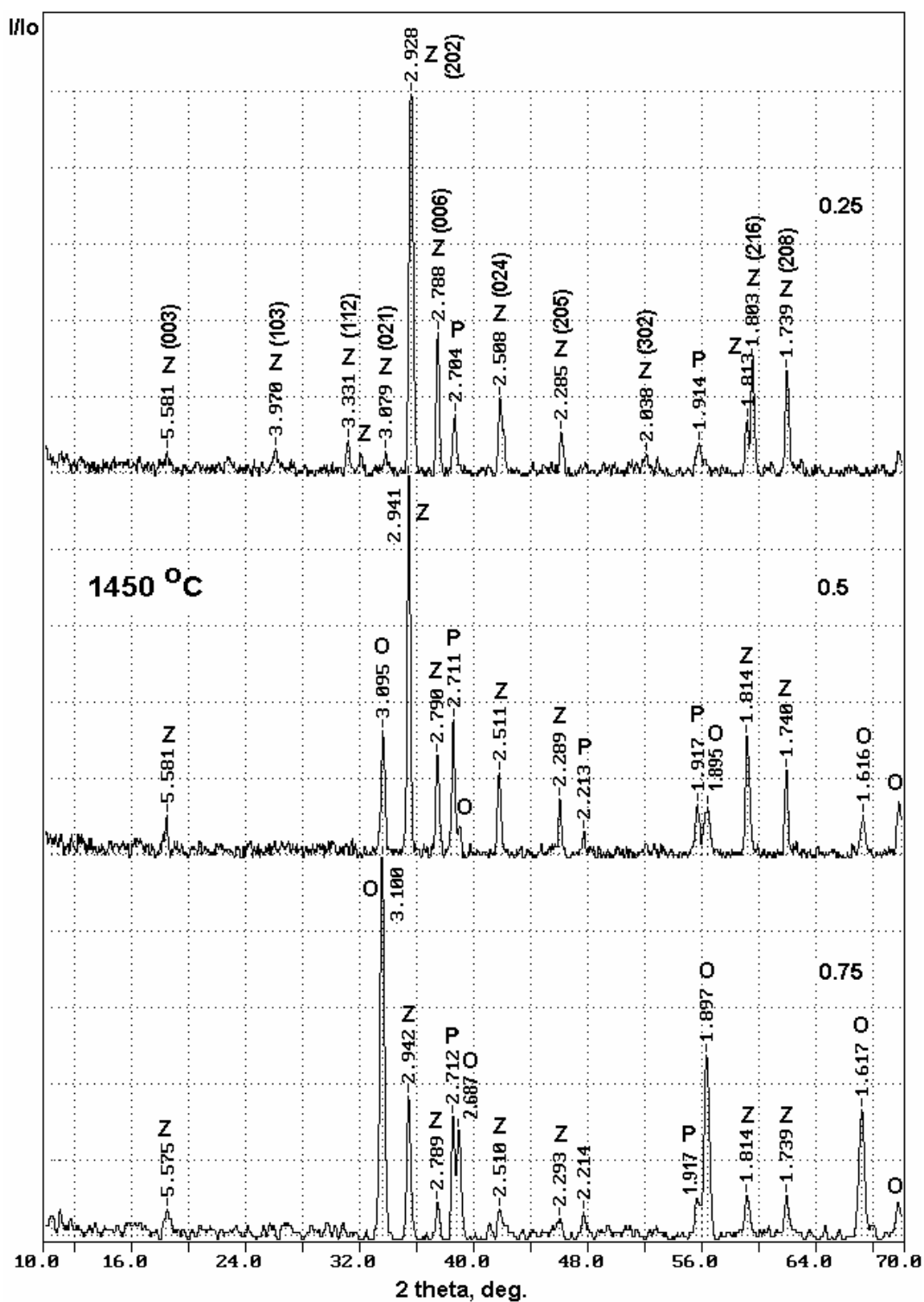


Fig. 2. XRD patterns of the ceramics in the series  $(1-x)\text{CaZrTi}_2\text{O}_7 - x\text{CeAlO}_3$  produced by sintering of pelletized oxide mixtures at  $1450\text{ }^\circ\text{C}$ .

O – oxide phase, P – perovskite structure phase, Z – zirconolite.

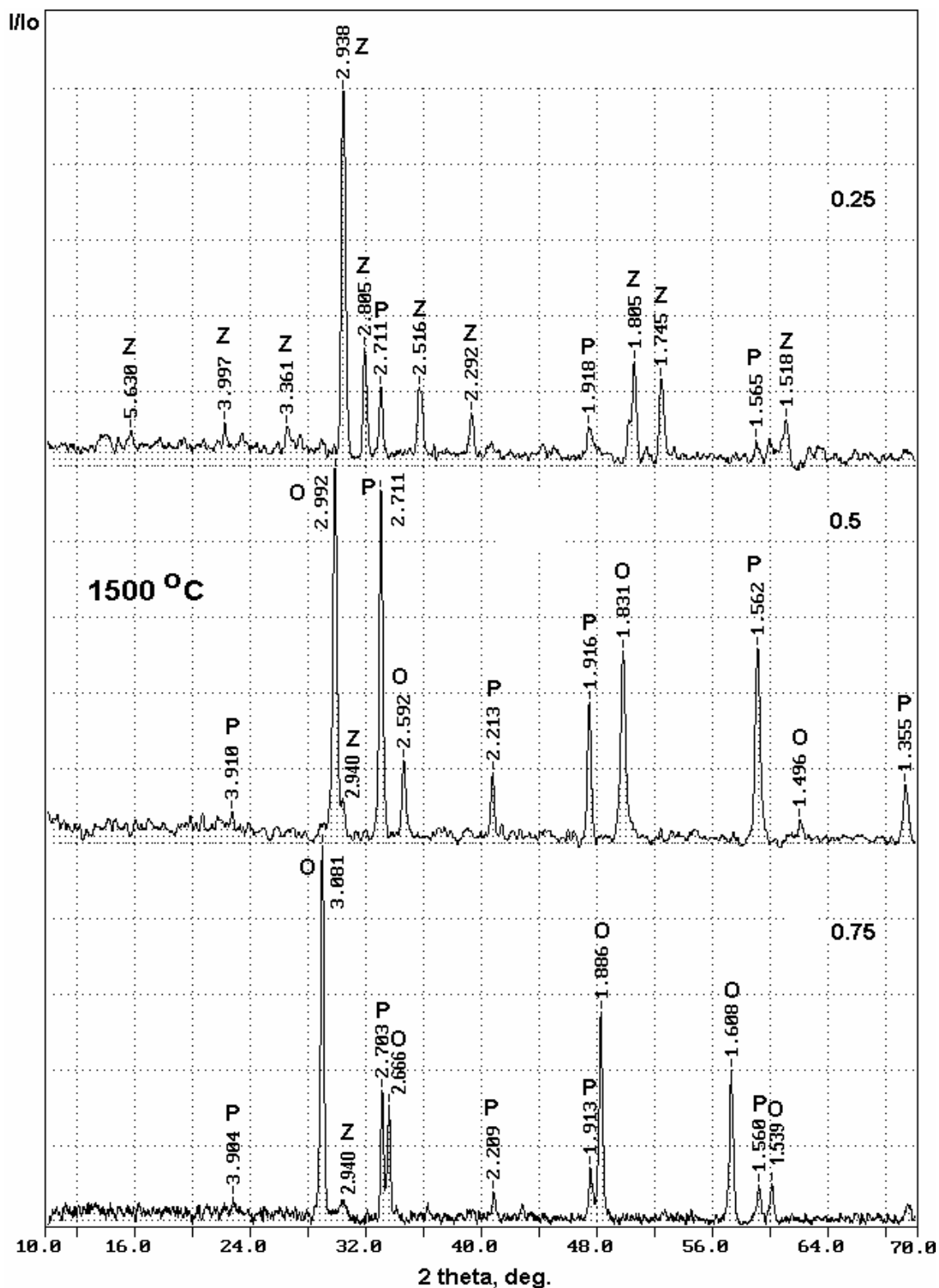


Fig. 3. XRD patterns of the ceramics in the series  $(1-x) \text{CaZrTi}_2\text{O}_7 - x \text{CeAlO}_3$  produced by sintering of pelletized oxide mixtures at 1500 °C.

O – oxide phase, P – perovskite structure phase, Z – zirronolite.

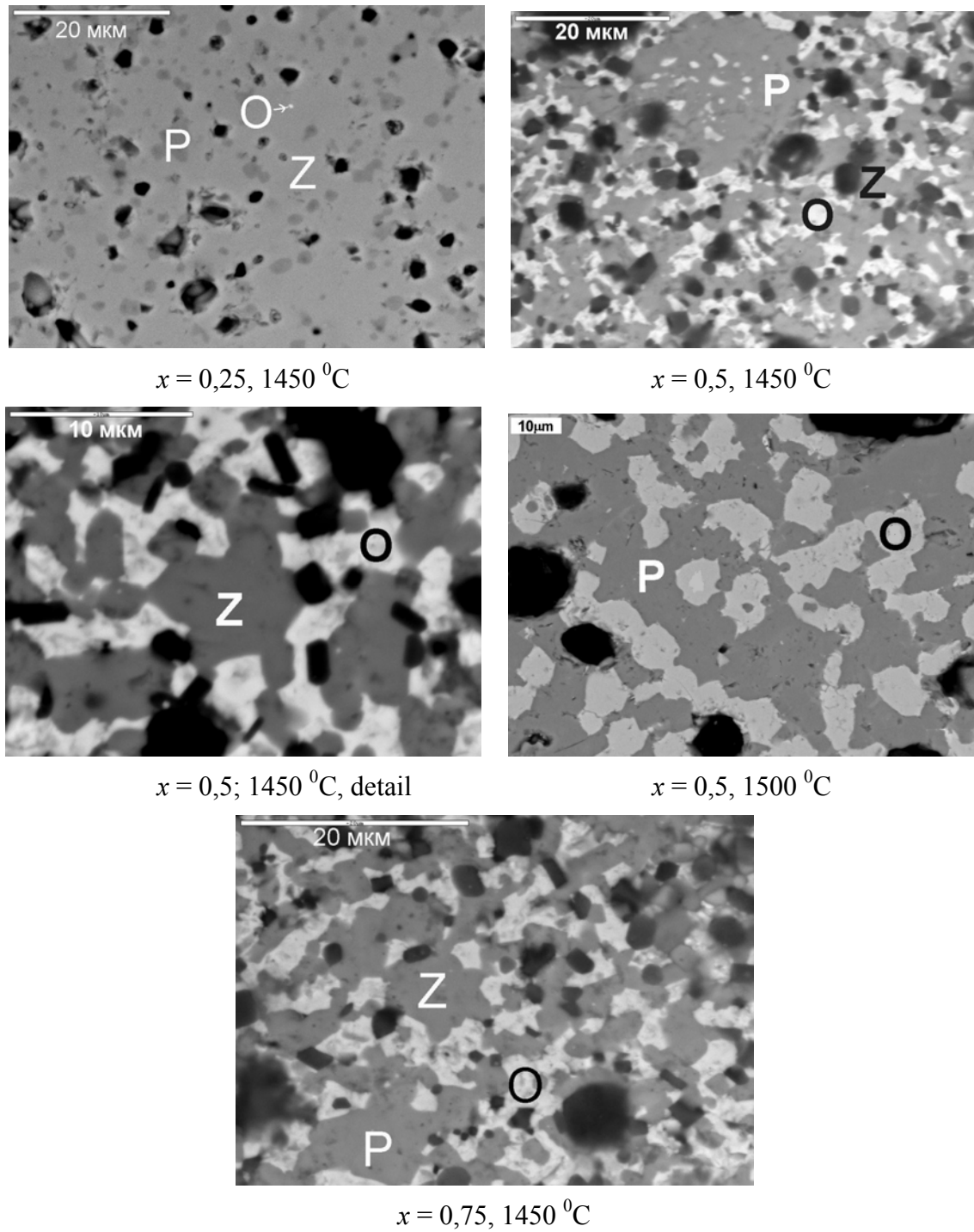


Fig. 4. SEM-images of the ceramics in the series  $(1-x)\text{CaZrTi}_2\text{O}_7 - x\text{CeAlO}_3$  produced by sintering of pelletized oxide mixtures at various temperatures.

O – oxide phase, P – perovskite structure phase, Z – zirconolite.

In the ceramics with equal target amounts of “zirconolite” and “perovskite” ( $x = 0.5$ ) sintered at 1400 and 1450 °C three phases co-exist: zirconolite (55-60% in each sample), oxide phase (20-25%), and perovskite (15-20%). The ceramic prepared at 1450 °C is composed on SEM-image of major gray-colored bulk with chemical composition corresponding to zirconolite with average formula  $\text{Ca}_{0.64}\text{Ce}_{0.49}\text{Zr}_{0.96}\text{Ti}_{1.48}\text{Al}_{0.45}\text{O}_7$  and light-gray perovskite grains ( $\text{Ca}_{0.52}\text{Ce}_{0.20}\text{Ti}_{0.88}\text{Zr}_{0.02}\text{Al}_{0.18}\text{O}_3$ ) and white grains with cerianite formulation ( $\text{Ce}_{0.75}\text{Zr}_{0.19}\text{Ti}_{0.02}\text{Ca}_{0.02}\text{Al}_{0.02}\text{O}_{1.97}$ ) distributed within (Figure 4).

Table I. Chemical composition (wt.%) of the ceramics in the series  $(1-x)\text{CaZrTi}_2\text{O}_7 - x\text{CeAlO}_3$  ( $x$  – molar fraction)

Oxides	$x=0.25, 1450\text{ }^\circ\text{C}$		$x=0.5, 1450\text{ }^\circ\text{C}$			$x=0.5, 1500\text{ }^\circ\text{C}$		$x=0.75, 1450\text{ }^\circ\text{C}$		
	Z	P	Z	P	O	P	O	Z	P	O
$\text{Al}_2\text{O}_3$	3.84	2.88	6.11	4.84	0.98	5.83	0.12	6.49	5.53	1.53
CaO	12.96	24.98	9.87	15.93	0.70	21.36	4.54	10.60	13.44	0.52
$\text{TiO}_2$	35.87	46.12	31.82	37.92	1.05	37.50	4.77	31.56	32.47	1.11
$\text{ZrO}_2$	36.05	2.62	32.40	0.93	14.88	1.56	64.13	33.65	4.18	13.61
$\text{Ce}_2\text{O}_3$	11.44	22.89	19.74	36.24	81.09	30.70	26.84	19.24	43.81	79.65
Total	100.15	99.49	99.94	95.86	98.70	96.95	100.40	101.53	99.44	96.42

Z – zirconolite, P – perovskite, O – oxide.

In the sample sintered at 1500 °C qualitative and quantitative phase compositions are strongly different (Figures 3 and 4). Major phases were found to be perovskite and fluorite structure oxide phase because no superstructure reflections typical of the pyrochlore lattice are observed on XRD patterns. Weak reflection at 2.940 Å is likely due to zirconolite. Thus for the ceramic with the given composition zirconolite is probably intermediate phase. However the effect of redox conditions when cerium is reduced to trivalent state at high temperatures and becomes a stabilizer for cubic lattice of zirconium dioxide with formation of cubic fluorite structure solid solution  $(\text{Zr}^{4+}_{1-x}\text{Ce}^{3+}_x)\text{O}_{2-0.5x}$  may be essential. SEM images of the ceramic with  $x = 0.5$  synthesized at 1500 °C demonstrate occurrence of lighter and darker sections (Figure 4). Chemical composition (Table I) of lighter phase is recalculated well to a formula with three oxygen anions and corresponds to perovskite:  $\text{Ca}_{0.64}\text{Ce}_{0.32}\text{Zr}_{0.02}\text{Ti}_{0.78}\text{Al}_{0.19}\text{O}_3$ . Darker-colored sections are composed of complex Ce-Zr-oxide with traces of Ti and Ca and formula  $\text{Ce}_{0.20}\text{Zr}_{0.65}\text{Ti}_{0.08}\text{Ca}_{0.07}\text{O}_{1.93}$  (natural analog is tazheranite [8]).

At  $x = 0.75$  in all three samples sintered at 1400, 1450, and 1500 °C complex fluorite structure oxide was found to be major phase. However if in the ceramics sintered at 1400 and 1450 °C zirconolite (secondary in abundance phase - ~30-35% of total bulk) and perovskite (minor phase - ~10-15%) are also present, then the ceramic sintered at 1500 °C doesn't almost contain zirconolite but fractions of oxide and perovskite may be evaluated as ~75% and ~25%, respectively. Chemical compositions of the phases (Table I) in the ceramic sintered at 1450 °C are recalculated well to averaged formulae:  $\text{Ce}_{0.75}\text{Zr}_{0.17}\text{Ti}_{0.02}\text{Ca}_{0.02}\text{O}_{1.98}$  (oxide),  $\text{Ca}_{0.68}\text{Ce}_{0.44}\text{Zr}_{1.00}\text{Ti}_{1.44}\text{Al}_{0.48}\text{O}_7$  (zirconolite), and  $\text{Ca}_{0.45}\text{Ce}_{0.35}\text{Ti}_{0.67}\text{Al}_{0.33}\text{O}_3$  (perovskite).

As follows from XRD data (Figures 1-3) chemical composition of the cubic fluorite structure solid solution at  $x = 0.5$  and  $x = 0.75$  is close to cerianite and is enriched with Zr at increase of synthesis temperature. It is seen well from shift of interatomic distances of the lattice of the

oxide phase towards reduction, for example, at  $x = 0.75$  for  $d_{111}$  – from 3.108 Å at 1400 °C to 3.081 Å at 1500 °C; at  $x = 0.5$  – from 3.106 Å at 1400 °C to 2.992 Å at 1500 °C. Such compositional variations are consistent with SEM/EDS data as well (Table I).

Note that the samples synthesized at 1500 °C have more differences from the samples prepared at lower temperatures. If in the ceramics sintered at 1400 and 1450 °C with increase fraction of perovskite constituent (increase  $x$  value from 0.25 to 0.75) zirconolite fraction gradually reduces at increase of oxide fraction, then in the ceramic kept at 1500 °C already at  $x = 0.5$  zirconolite fraction becomes extremely low (<5%) with simultaneous strong increase of perovskite fraction whose content becomes comparable with the oxide phase content. In the ceramics sintered at 1400 and 1450 °C increase of  $x$  value results in gradual minor changes in chemical composition of the oxide phase towards enrichment with Ce (shift of major reflection from 3.092 Å for the sample with  $x = 0.25$  to 3.108 Å for the sample with  $x = 0.75$  at 1400 °C and from 3.079 Å for the sample with  $x = 0.25$  to 3.100 Å for the sample with  $x = 0.75$  at 1450 °C) but in the sample with  $x = 0.25$  synthesized at 1500 °C oxide phase content is negligible. In the sample with  $x = 0.5$  this phase is strongly enriched with Zr and it significantly different in chemical composition from the oxide phase in the samples sintered at lower temperatures. In the sample with  $x = 0.75$  oxide phase becomes Ce-rich again. On XRD patterns of the ceramics with  $x = 0.25$  shift of major diffraction peaks due to zirconolite to higher angles at increase of synthesis temperature from 1400 °C ( $d_{221} = 2.941$  Å) to 1450 °C ( $d_{221} = 2.928$  Å) was observed but in the ceramic prepared at 1500 °C major zirconolite reflection is shifted to lower angles again and positioned at 2.938 Å.

The changes observed should be connected to variations of redox conditions at increase of temperature in the system. At moderate temperatures significant Ce fraction is in tetravalent state and enters zirconolite and perovskite. The rest of Ce (both tri- and tetravalent) is located in perovskite. At increase of sintering temperature from 1400 to 1500 °C fraction of trivalent Ce grows and tetravalent reduces but at 1450 °C amount of Ce(III) is minor. At relative low content of perovskite constituent ( $x = 0.25$ ) this doesn't affect markedly phase composition of the samples because Ce introduced with the latter is partitioned between zirconolite and perovskite – both the phases have isomorphic capacity enough for accommodation all the Ce introduced in the system. Different elements (Ca, Ti, Al) are partitioned among co-existing phases (Table I). But when fraction of the perovskite constituent becomes significant ( $x = 0.5$  or  $x = 0.75$ ) isomorphic capacity of the zirconolite with respect to Ce(IV) is not enough to accommodate all the Ce and therefore fractions of both perovskite and particularly cubic fluorite structure cerianite-based solid solution are increased. However, within the temperature range between 1450 °C and 1500 °C redox equilibrium is shifted towards significant increase of Ce(III) fraction and at high nominal perovskite content all the Ce(III) is partitioned among perovskite and cubic zirconia-based solid solution. At  $x = 0.75$  all the Ce is partitioned between cerianite-based oxide and perovskite.

XRD pattern of the zirconolite in the Ce-bearing samples at  $x = 0.25$  demonstrates clear trace of “hexagonalization” (Figures 1-3), i.e. unlike XRD pattern of the zirconolite with nominal composition ( $\text{CaZrTi}_2\text{O}_7$ ) some superstructure reflections disappear pointing to transformation of the monoclinic zirconolite-2M structure to the structure with higher symmetry supposedly trigonal (zirconolite-3T or 6T). Zirconolite lattice parameters in the samples studied in suggestion of trigonal (hexagonal) lattice symmetry are given in Table II. Miller's indices (in brackets) for hexagonal lattice of zirconolite-3T (zirkelite) with space group  $P3_121$  [9] are also



given on Figure 1. Results of indexing of XRD peaks demonstrated good agreement with reference data.

Table II. Unit cell parameters of the zirconolite phase in suggestion of its trigonal symmetry

T, °C	x, f.u.	a, Å	b, Å	c, Å	$\angle\beta$ , deg.	Formula
1400	0.25	7.252	7.252	16.788	90.00	Not determined
	0.5	7.263	7.263	16.734	90.00	Not determined
	0.75	7.264	7.264	16.716	90.00	Not determined
1450	0.25	7.219	7.219	16.728	90.00	Ca <sub>0.81</sub> Ce <sub>0.24</sub> Zr <sub>1.05</sub> Ti <sub>1.60</sub> Al <sub>0.28</sub> O <sub>7</sub>
	0.5	7.255	7.255	16.740	90.00	Ca <sub>0.64</sub> Ce <sub>0.49</sub> Zr <sub>0.96</sub> Ti <sub>1.48</sub> Al <sub>0.45</sub> O <sub>7</sub>
	0.75	7.258	7.258	16.734	90.00	Ca <sub>0.68</sub> Ce <sub>0.44</sub> Zr <sub>1.00</sub> Ti <sub>1.44</sub> Al <sub>0.48</sub> O <sub>7</sub>
1500	0.25	7.241	7.241	16.830	90.00	Not determined

It is also seen from Table II that if to compare elementary unit cell parameters of the zirconolite phase in the ceramics synthesized at certain temperatures (1400 and 1450 °C) then in the ceramic sintered at 1400 °C increase of  $x$  value, and therefore Ce content in zirconolite, increase of the zirconolite unit cell dimension along the  $a$  and  $b$  axes is accompanied by decrease of the  $c$  parameter, i.e. higher symmetry takes place. In the ceramic sintered at 1450 °C the zirconolite unit cell parameters increase with  $x$  value increase from 0.25 to 0.5 following by symmetrization at  $x = 0.75$ . The reason of this behavior is probably due to features of phase composition and elemental distribution between the phases. As follows from Table I at  $x = 0.5$  Ce content in zirconolite achieves maximum (~20 wt.% or 0.49 fu) and at  $x = 0.75$  even slightly decreases (0.44 fu). This results in corresponding variations in elementary unit cell dimensions as well.

Interphase elemental partitioning in the Ce-bearing ceramics is given in Table III. At low  $x$  values zirconolite is major host phase for both Ce and Zr. Zirconolite accumulates about  $\frac{3}{4}$  of total Ce and almost all Zr. In the ceramics with low zirconolite content Ce preferably enters zirconia or cerianite-based phase where it is present in tetravalent form and Zr enters either cubic fianite-type oxide or is partitioned among zirconolite and ceria-zirconia solid solution.

Table III. Oxides partitioning among co-existing phases in the ceramics of the series  $(1-x)\text{CaZrTi}_2\text{O}_7 - x\text{CeAlO}_3$  sintered at 1450 and 1500 °C

T, °C	$x$	Phase	Fraction, %	Al <sub>2</sub> O <sub>3</sub>	CaO	TiO <sub>2</sub>	ZrO <sub>2</sub>	Ce <sub>2</sub> O <sub>3</sub>
1450	0.25	Zirconolite	85	87	75	82	99	74
		Perovskite	15	13	25	18	1	26
1500	0.5	Perovskite	45	>99	80	87	2	48
		Oxide	55	<1	20	13	98	52
1450	0.75	Perovskite	20	31	47	43	5	15
		Zirconolite	25	45	47	53	50	8
		Oxide	55	24	6	4	45	77

## CONCLUSION

Actual phase composition of the ceramics formally related to the pseudo-binary system  $\text{CaZrTi}_2\text{O}_7 - \text{CeAlO}_3$  (zirconolite-perovskite) at rather high content of perovskite constituent is more complicated due to formation of cerianite-based oxide phase that effects appreciably on cerium partitioning. Amount of this phase increases with increase of sintering temperature (up to  $1500^\circ\text{C}$ ) and it becomes predominant in the ceramic with nominally equal fractions of zirconolite and perovskite constituents accumulating of about 77% of total Ce in the sample. At the same time at significant predominance of the zirconolite constituent (75% by calculation) it accumulates almost  $\frac{3}{4}$  of total cerium introduced

## ACKNOWLEDGEMENTS

The work was performed under financial support of US DOE (Project RUC2-20009-MO-04).

## REFERENCES

1. Yu.L. Kapustin, N.M. Chernitsova, and Z.V. Pudovkina, Minerals and Paragenesis of Minerals and Rocks (Russ.) Leningrad, USSR, Nedra (1973) 17-25.
2. E.R. Vance, P.J. Angel, B.D. Begg, and R.A. Day, Mat. Res. Soc. Symp. Proc. **333** (1994) 293-298.
3. E.R. Vance, B.D. Begg, R.A. Day, and C.J. Ball, Mat. Res. Soc. Symp. Proc. **353** (1995) 767-774.
4. B.D. Begg and E.R. Vance, Mat. Res. Soc. Symp. Proc. **465** (1997) 333-340.
5. N.P. Laverov, S.V. Yudintsev, S.V. Stefanovsky, Y.N. Jang, and R.C. Ewing, Mat. Res. Soc. Symp. Proc. **713** (2002) 337-344.
6. S.V. Stefanovsky, S.V. Chizhevskaya, A.S. Mironov, O.I. Kirjanova, and S.V. Yudintsev, Adv. Mater. (Russ.) [6] (2003) 61-68.
7. J.A. Fortner and E.C. Buck, Appl. Phys. Lett. **68** (1996) 3817-3819.
8. R.K. Rastsvetaeva, D.Yu. Pushtcharovsky, E.M. Spiridonov and V.M. Gekimiantz, Acad. Sci. Rep. (Russ. – Doklady Akademii Nauk) **359** (1998) 529-531.
9. F. Mazzi, R. Munno, Amer. Miner. **68** (1983) 262-276.